A STUDY OF ANOMALOUS HALL AND NERNST EFFECT IN $L2_1$ HUESLER ALLOY

A DISSERTATION

SUBMITTED IN PARTIAL FULFILLMENT OF THE REQUIREMENTS FOR THE AWARD OF THE DEGREE OF

MASTER OF SCIENCE IN PHYSICS

Submitted by:

SATYAM VERMA

2K24/MSCPHY/62

Under the supervision of

Dr. MUKHTIYAR SINGH

Assistant Professor

DEPARTMENT OF APPLIED PHYSICS

DELHI TECHNOLOGICAL UNIVERSITY

(Formerly Delhi College of Engineering) Bawana Road, Delhi-110042

May, 2026

DELHI TECHNOLOGICAL UNIVERSITY

(Formerly Delhi College of Engineering)

Bawana Road, Delhi-110042

CANDIDATE'S DECLARATION

I **SATYAM VERMA**, Roll No. **2K24/MSCPHY/62** student of **M.Sc. (Physics)**, hereby declare that the project Dissertation titled **"A STUDY OF ANOMALOUS HALL AND NERNST EFFECT IN $L2_1$ HUESLER ALLOY**", which is submitted by me to the **Department of Applied Physics, Delhi Technological University, Delhi** in partial fulfilment of the requirement for the award of the degree of Master's in Physics is original and not copied from any source without proper citation. This work has not previously formed the basis for awarding any Degree, Diploma Associateship, Fellowship, or other similar title or recognition.

The work has been under review in a peer-reviewed Scopus-indexed conferen -ce with the following details:

Title of Paper: "**Berry curvature driven Anomalous transport behaviour in Ferromagnetic Co_2CrAs and Co_2CrSb Heusler alloys**"

Authors' names (in sequence as per research paper): Satyam Verma, Kulwinder Kumar, and Mukhtiyar Singh.

Name of conference / Journal: National Conference on Emerging Trends in Multifunctional Materials and Devices (NC-ETMMD-2026)

Have you registered for conference (Yes/No): Yes

Status of paper (Accepted/Published/comment): comment

Date of communication: April 2, 2025

Date of acceptance: Yet to be accepted

Date of publication: Yet to be published

Satyam

Place: Delhi **SATYAM VERMA**

Date: 28/05/2026 **(2K24/MSCPHY/62)**

This is to certify that the student has incorporated all the corrections suggested by the examiners in the thesis and that the statement made by the candidate is correct to the best of our knowledge.

28/05/26

DR. MUKHTIYAR SINGH
Supervisor
(Assistant Professor)

ACKNOWLEDGEMENT

I would like to express my deepest sincere gratitude to my supervisor, **Dr. Mukhtiyar Singh**, Assistant Professor, **Department of Applied Physics, Delhi Technological University** for allowing me to work under his guidance and for constant inspiration and incessant support throughout the project. I take this opportunity to express our indebtedness to my supervisor for his enthusiastic help, expertise, brilliant ideas, valuable suggestions, and constant encouragement. I am grateful to acknowledge the constant help and convenience at every step of our project by all the lab members (PhD scholar Mr. Kulwinder Kumar), Dept. of Applied Physics. Lately, I am thankful to our families and friends for their love, care, and support who patiently extended all sorts of help for accomplishing this task.

Satyam

SATYAM VERMA
(2K24/MSCPHY/62)

ABSTRACT

In the application of efficient materials, including spintronics devices, magnetic field sensors, storage devices, and waste heat energy recovery systems, the anomalous transport phenomena play a crucial role. The anomalous transport, including the AHE and ANE are driven by Berry curvature, which is a geometrical property of SOC electronic bands in the magnetic materials. The Present study utilized the ab- initio calculation method to explore the AHE and ANE in the Co_2CrAs and Co_2CrSb types of Co-based Ferromagnetic Heusler alloys, with magnetic moment of 5 μ_B. The net magnetization oriented along the [001] direction, the major Berry curvature originates from specific electronic states lying at the Fermi energy in the bandstructure under the SOC effect. The overall large Berry curvature further leads to the large AHC and ANC with values 584.38 (-668.99) Scm-1 and -4.71 (-2.68) $Am^{-1}K^{-1}$, for Co_2CrAs (Co_2CrSb) Heusler alloy. The pronounced anomalous transport responses obtained for Co_2CrAs and Co_2CrSb Heusler alloys suggest that these materials could serve as promising candidates for emerging quantum technologies and thermoelectric applications.

Table of Contents

LIST OF FIGURES

LIST OF TABLES

LIST OF SYMBOLS AND ABBREVIATIONS

TSM	Topological semimetal
E_F	Fermi level
IS	Inversion symmetry
TRS	Time reversal symmetry
AHE	Anomalous Hall Effect
ANE	Anomalous Nernst Effect
AHC	Anomalous Hall Conductivity
ANC	Anomalous Nernst Conductivity
GGA	Generalized gradient approximation
SOC	Spin orbit coupling
VASP	Vienna ab initio simulation package
DFT	Density Functional Theory

CHAPTER 1

INTRODUCTION

Over the last decade, the material science community has shown growing interest in materials with strong Anomalous Transport behaviour driven by their applicability in spintronics, energy conversion, sensing, and quantum devices [1–3]. Anomalous transport phenomena primarily encompass the anomalous Hall effect (AHE) and the anomalous Nernst effect (ANE), both of which arise independently of the conventional Lorentz-force mechanism associated with an external magnetic field [4]. The AHE is results of the appearance of a transverse voltage generated by a longitudinal charge current as a consequence of intrinsic magnetization.

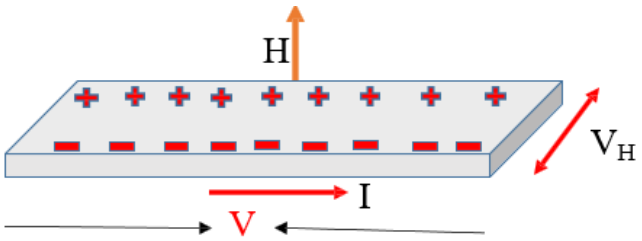

Figure 1: Anomalous Nernst effect (ANE)[5].

In contrast, the ANE represents the thermoelectric analogue of the AHE, where a temperature gradient in a magnetic material produces a transverse electrical response [5].

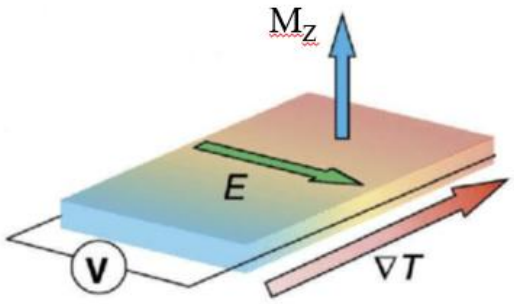

Figure 2: Anomalous Nernst effect (ANE)[5].

Despite the traditional Seebeck effect-based thermoelectric (TE) phenomenon, ANE based TE device overcomes the limited device connection complications and also provides large TE efficiency [1,6,7]. AHE and ANE are most popular Anomalous Transport Phenomena, which are exciting because their origin is internal magnetic field instead of external magnetic field. A quantum transport phenomenon where electric current flows through magnetic material, giving a perpendicular voltage without applying an external magnetic field, is known as the AHE [8-9], Which is differ from the conventional Hall effect. This phenomenon arises due to magnetism's complex interplay, spin-orbit coupling, and scattering mechanism. The fundamental microscopic mechanism underlying anomalous transport phenomena remains an active topic of investigation. The foundation of AHE origin was first mentioned in the work of Karplus and Luttinger in the 1905s, which describes intrinsic contributions that do not depend on scattering and extrinsic mechanisms introducing asymmetrical impurity scattering [8-10]. Within the Karplus–Luttinger framework, these effects are explained as intrinsic responses originating from spin–orbit coupling and spontaneous magnetization, mediated by the Berry curvature of the electronic band-structure [8,9]. Berry curvature is a geometric characteristic of coupled electronic bands that behaves

like an effective magnetic field in momentum space and plays a central role in generating anomalous transport responses [10]. It changes sign under time-reversal symmetry while remaining invariant under spatial inversion. Consequently, a finite net Berry curvature can arise only when time-reversal symmetry, inversion symmetry, or both are broken [11]. Magnetic materials naturally exhibit the TRS breaking, and the non-centrosymmetric systems have breaking IS, which might be the ideal candidate for the study of the Anomalous transport phenomena [12,13].

1.1 Literature review

Quantum phenomena like Anomalous Transport phenomena (ATP) have attracted researcher due to huge application in spintronics, Sensors And quantum technologies. Initially, scientists believed that this phenomenon was directly proportional to the magnetization of material, but recent theory says that they originate from the Berry curvature of electric bands near the Fermi levels [10]. This effect was observed in many materials, and topological materials are potentially remarkable [14].

In this sequence, Nagaosa et al. [4] predicted a giant anomalous hall transport in magnetic materials. His work clarified role of berry curvature in calculating hall conductivity. Further Xiao et al. [15] confirmed in momentum space Berry curvature is an effective magnetic field, which influences electron transport in materials. Berry curvature had many unconventional transport responses due to which this is one of the important factors to explore topological properties of materials. As it remains invariant under inversion symmetry, and change sign under time-reversal symmetry, finite Berry curvature require breaking of at least one or both symmetries. Therefore,

magnetic and non-centrosymmetric compounds are ideal system for anomalous transport phenomenon.

Heusler alloys are the promising candidates, show topological property like Anomalous Transport property due to their half-metallicity, large Curie temperature and large spin polarization. Many research work of scientists have reported huge AHC and ANC in Co-based Heusler alloys driven by Berry curvature.

Guin et-al, [16] experimentally explore the AHC and the ANC of ferromagnetic Heusler alloys, their work mainly focused on Berry curvature near fermi level generate high transport coefficients. And magnitude of the AHC and the ANC depend on electronic topology. While Noky et al. [18] predicted Berry-Curvature-driven transport behaviour of many magnetic alloys by first- principle. The conclusion of their work is topological band and Weyl nodes crossing near fermi-level show better transport properties. And focus on importance of symmetry breaking and spin-orbit coupling to generate large Berry curvature.

Several study have done to explore transport properties in Co-based Heusler Alloys. Kakti et al. [20] predict magnetic properties and topological properties in Heusler Alloys and reported that transport response depend on electronic band structure. Chatterjee et al. study of magnetic system demonstrate that Berry curvature distribution can be enhanced by breaking of symmetry. Wang et al. [21] thoroughly studied the existence of nodal lines and the Weyl points in the Co_2ZrSn full Heusler system using first-principles calculation. Co_2MnGe Heusler alloy has been predicted to exhibit the multiple Weyl cone in the band structure. Chang et al. [22] analysed the nodal line and Weyl points in the Co2TiX (X= Si, Ge or Sn) using the first

principles calculation. Recently, a giant AHC of about 1600 S/cm has been observed in the Co2MnAl ferromagnetic topological semimetal [23]. This large AHE in Co_2MnAl is attributed to the presence of nodal rings and Weyl points near the Fermi energy. Another well-known system is Co_2MnGa Heusler alloy which is reported to show large AHC and ANC about 1200 S/cm and 4.0 A/m-K gue to the gapped nodal lines near the Fermi energy [24]. The large AHE and ANE are theoretically reported in the Co_2FeGe Heusler alloy above 100 meV to the Fermi level due to the SOC-induced nodal line symmetry breaking [25-26]. Very recently, our group theoretically predicted a large AHC of about 1000 S/cm in the Cu_2CoSn, where the gapping in the nodal line creates large Berry curvature at the Fermi surface [27]. Considering the potential of the Co-based Heusler alloys as the topological semimetal with large anomalous transport response, high Curie temperature, and high-spin polarization, makes these systems potential candidates for spintronic applications [28-30]. These materials carry the magnetic properties without any magnetic entity, which makes them a possible candidate for the study of Anomalous transport. Heusler alloys are classified as Half Heusler and Full Heusler alloys based on their chemical composition. If the composition is XYZ with a 1:1:1 stoichiometry, then it's a Half Heusler alloy, and if X_2YZ with a 2:1:1 stoichiometry, where the transition metals are X and Y, and Z is a main group element [17]. Recently, Guin et al. experimentally and theoretically predicted a giant AHC and ANC in a Co-based Full Heusler alloy [18]. Although numerous studies on magnetic Heusler alloys exist in the literature, only a limited number address the TRS breaking criterion linked with Berry curvature and the associated anomalous transport behaviour [13,18–25].

We are interested in investigating Co-based Heusler alloys, focusing on topological

semimetals for large anomalous transport responses. The Berry curvature arising from the topologically protected bands in these materials leads to pronounced anomalous Hall and Nernst effects. The AHE holds potential for spintronics applications, such as nanoscale read head sensors, high-frequency Hall sensors, memory devices, etc. Additionally, the ANE could enable more efficient conversion of heat into electricity compared to traditional thermoelectric materials.

Co_2CrAs and Co_2CrSb are types of Co-based magnetic full Heusler alloys, which were theoretically predicted both materials as Ferromagnetic half Metallic system by Kanbur et al. [26]. However, some other studies also present in the literature on these alloys consider only the effect of pressure and temperature, and mostly are focused on the half-metallic feature [27,28]. But no one has yet explored their Anomalous transport behaviour, led by the Berry curvature feature. To fill this gap, motivated by this, this study systematically presents a computational prediction of the Berry curvature-driven AHE and ANE in the Magnetic Heusler alloys.

CHAPTER 2

METHODOLOGY

The study of Anomalous Transport properties was done using DFT-based first-principles calculations. The calculations were performed using VASP with the projector augmented wave (PAW) method and generalized gradient approximation(GGA) for exchange-correlation effects [31]. Structural optimization was followed by analysis of mechanical stability through the calculation of elastic constants. Electronic properties were studied by calculating band structures and density of states. To examine topological characteristics, spin-orbit coupling (SOC) was included in band structure calculations. The anomalous transport properties were calculated via Wannier charge center evolution by employing Wannier90 and WannierTools [32-33]. All computational tools employed in this study include VASP, Wannier90 and Wannier tool. In the following sections, the computational methods and packages are discussed in detail.

2.1 Density Functional Theory (DFT)

The density functional based method is one of the most popular theoretical methods for electronic properties of materials at the atomic level. It is the backbone of contemporary computational condensed matter physics and material science. The approach is the principle that ground-state of an interacting many-electron system can be fully specified by its electron density, as opposed to the complicated many-body wave function. The basic thought behind this method is the mapping of a complicated many-body problem into an easier one by taking recourse to a system of non-

interacting electrons that have the same electron density as the interacting system in question. This mapping considerably eases the computational complexity at the expense of none of the important physics. This theoretical concept became feasible with the advent of the Kohn-Sham (KS) formulation, which gives a means to solve for the ground-state electron density through the use of self-consistent field methods [34]. The KS equations are a collection of single-particle equations that are simpler to solve numerically. The validity of this approach is highly dependent on the proper modelling of the exchange-correlation energy, a phrase that describes the quantum mechanical interactions between electrons, such as their mutual repulsion and quantum exchange effects. In the KS version of DFT, the many-electron problem of interacting electrons is solved by a set of non-interacting electrons defined in terms of the following self-consistent equations:

$$-\hbar^2/2m\,\nabla^2 + V_{eff}(r)\,\Psi_i(r) = \varepsilon_i\Psi_i(r) \tag{2.1}$$

Here $\Psi_i(r)$ are the KS orbitals, ε_i - the associated eigenvalues and $V_{eff}(r)$ - the effective potential, given by:

$$V_{eff}(r) = V_{ext}(r) + V_H(r) + V_{xc}(r) \tag{2.2}$$

Here $V_{ext}(r)$ - external potential, $V_H(r)$ - the Hartree Potential and $V_{xc}(r)$ - the exchange correlation potential. The electron density is derived from Kohn–Sham orbitals as:

$$n(r) = \Sigma_i^{occ}|\Psi_i(r)|^2 \tag{2.3}$$

These equations are then solved iteratively until self-consistency is established that is, until input and output electron densities agree. Over the last few decades, the

density functional based method has been extremely successful in the prediction of a broad spectrum of material properties such as structural stability, electronic band structure, magnetic ordering, and even topological features. It is especially useful for the investigation of new materials like topological insulators, superconductors, and thermoelectric, where experimental information can be scarce or hard to obtain [35].

2.2 Exchange correlation functionals

The exchange-correlation functional is the key ingredient in DFT. It embodies the combined impact of exchange and correlation electron interactions that are two quantum mechanical effects that are difficult to represent accurately. As the precise form of this functional is not known for the majority of real systems, several approximations have been formulated to render DFT computationally useful. The way the electron density and its spatial fluctuation are treated in these approximations varies, leading to a range of functionals with different strengths and limits. The Local Density Approximation (LDA), Generalized Gradient Approximation (GGA), and Hybrid Functionals are the most commonly utilized forms. Each has particular uses depending on the kind of system being studied.

2.2.1 Generalized Gradient Approximation (GGA)

The GGA is a development beyond LDA in that the electron density at every point and how it varies in space are taken into account. This permits GGA functionals to have a more realistic description of the behaviour of inhomogeneous electron systems, such that they can be more accurately used for molecules, surfaces, and transition metal

oxides. GGA fixes many of the deficiencies of LDA, making more accurate predictions of lattice parameters, cohesive energies, and magnetic properties. The most popular GGA functionals are the Perdew-Burke-Ernzerhof functionals [36]. GGA is usually regarded as the norm for most solid-state DFT calculations because it provides a good balance between accuracy and computational expense.

Perdew-Burke-Ernzerhof

The PBE functional is among the most popular GGA functionals. It is an improvement over the LDA since it includes the gradient of the electron density, enabling it to better handle inhomogeneities. In this study, PBE was selected for the exchange-correlation potential because of its compromise between computational cost and structural and electronic property reproduction accuracy. PBE is particularly accurate for the study of semiconductors and transition metal compounds, and is used in most conventional DFT codes, such as VASP [37].

2.3 Computational packages

2.3.1 VASP

The VASP is a tool employed for conducting quantum mechanical calculations. This involves the use of PAW, coupled with a plane wave basis set [38]. VASP solves the many-body Schrödinger equation approximately by solving the KS equation (in the framework of DFT) or by solving the Roothaan equations (in the framework of the Hartree-Fock approach). Additionally, certain hybrid functionals that inherit aspects from both the Hartree-Fock approach and the DFT are also available [39]. VASP calculates key quantities through a plane

wave basis: single-electron orbitals, charge density, and local potential. The exchange the electrons and ions is either expressed with the help of the PAW method or with the help of norm-conserving or ultrasoft pseudopotentials [40]. VASP carries out calculations using 4 necessary input files, which are

- **INCAR**: This file is used to determine what kind of calculation has to be done on the investigated system. There are certain tags specified in the INCAR file which we have to set to select a certain algorithm and set the parameters.
- **POSCAR**: This file gives the details of the system that we study. it consists of the atomic positions in the unit cell and the translational vectors.
- **POTCAR:** This file consists of the pseudopotential for every single atomic species which is present in Mendeleev's.
- **K-point sampling:** A crystalline solid is composed of unit cells with a periodic arrangement of atoms. The solid is initially transformed into a supercell with several unit cells to handle the full solid. After the supercell is expanded to infinity using the periodic boundary conditions, it is transformed into reciprocal space contained within the first Brillouin zone (BZ). We can further compress the BZ by using symmetry operations to transfer the entire solid to the irreducible Brillouin zone (IBZ). An endless number of wave functions can be produced by using k-vectors to represent the points in an IBZ. Each k-point contains information about the kinetic energy, direction, and amplitude of the wave vector at that specific location. Since it is nearly impossible to take

into account every k-point, DFT computations employ a small number of k-points utilizing the following schemes:

Monkhorst-Pack method: In order to determine the ground state energy, which is converged in DFT calculations for each system, Monkhorst and Pack presented a method in 1976 to create a homogeneous mesh of k-points sampled throughout the whole IBZ [41].

Γ-point: A large supercell can be fully described by a single point, which is described as Γ-point. Since it is the place where real and reciprocal spaces coincide, a real wave function will be employed [41-42].

2.3.2 Wannier90

Wannier90 is an open-source tool designed to construct maximally localized Wannier functions (MLWFs) from DFT outputs [32-33]. In this study, it played a crucial role in generating a tight-binding Hamiltonian that accurately reproduces the ab initio band structure, particularly near the Fermi level. The process started with the wannier.win file which defines the projections, number of bands, frozen and disentangled energy windows, and other parameters necessary for Wannierization. The wannier.eig file provided the band eigenvalues of VASP, while the wannier.mmn and wannier.amn files contained matrix elements and projection overlaps, respectively. These were necessary for the localization process and the formation of MLWFs. The output Wannier functions maintained the symmetry and character of the initial atomic orbitals but were spatially localized, which is very important in investigating topological properties.

2.3.3 WannierTool

WannierTools is a versatile software package employed to investigate the topological properties of materials based on tight-binding models extracted from Wannier90 [33]. In this paper, WannierTools was used to compute the Berry curvature, AHC and ANC. The fundamental input to these calculations is the wt.in file that sets a variety of computational parameters.

2.4 Summary

The study employed DFT using the VASP code with the PAW method and the PBE form of the GGA for exchange-correlation effects. Structural optimization, elastic constants, and electronic properties were evaluated, with SOC included to analyze topological features. Wannier90 was used to generate maximally localized Wannier functions and construct tight-binding models. WannierTools facilitated the computation of Anomalous transport properties. The methodology integrates electronic structure analysis and anomalous conductivites calculations through VASP, Wannier90, and WannierTools.

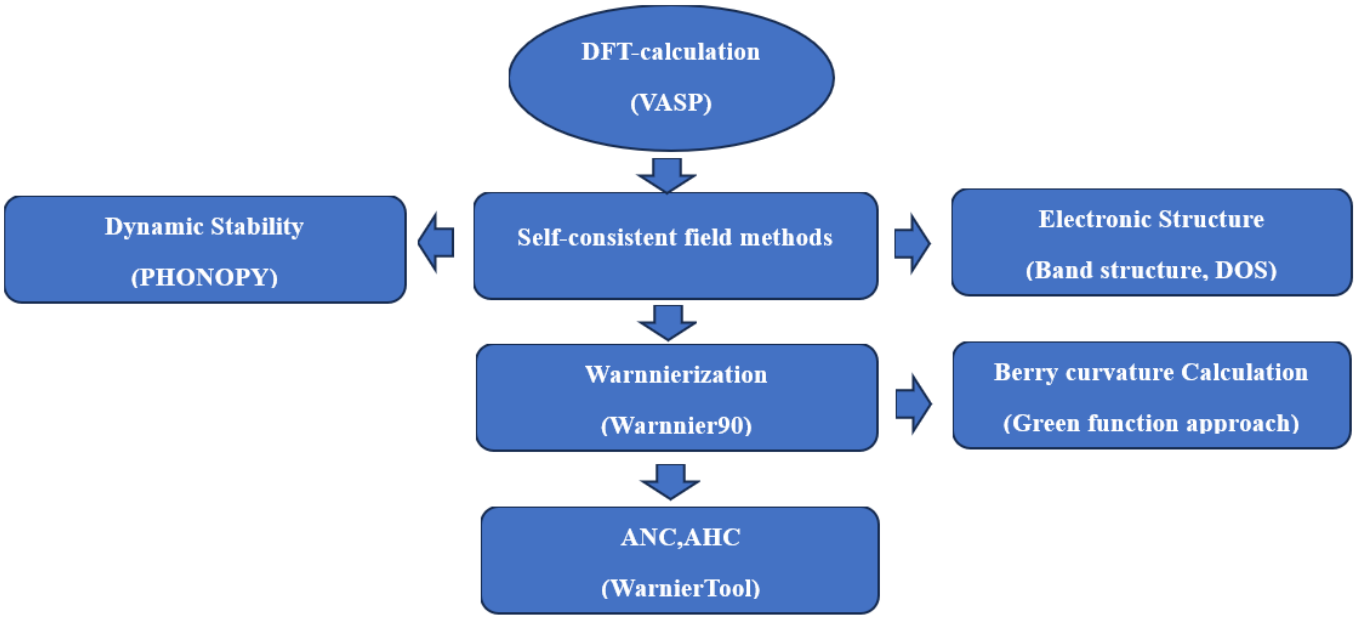

Figure 3: Schematic representation of the DFT-based workflow.

CHAPTER 3

BERRY CURVATURE DRIVEN ANOMALOUS TRANSPORT BEHAVIOUR IN FERROMAGNETIC HEUSLER ALLOYS

3.1 Introductions

In recent years, the material science community has shown growing interest in materials with strong Anomalous Transport behaviour driven by their applicability in spintronics, energy conversion, sensing, and quantum devices [5-8]. Anomalous Transport Phenomena mainly include the AHE and ANE, which are not driven by the Lorentz force in an external magnetic field. The AHE is results of the appearance of a transverse voltage generated by a longitudinal charge current as a consequence of intrinsic magnetization [12-15]. On the other hand, ANE is thermoelectric counterpart of AHE, which is characterised as a longitudinal current govern by temperature gradient in the magnetic materials. Despite the traditional Seebeck effect-based thermoelectric (TE) phenomenon, ANE based TE device overcomes the limited device connection complications and also provides large TE efficiency. The microscopic origin of the anomalous transport phenomena is not fully understood; however, the Karplus-Luttinger (KL) mechanism attributes it to intrinsic magnetism and spin-orbit coupling (SOC) through the Berry curvature of the electronic bands [8-9]. Berry curvature is a geometrical property of entangled electronic bands, which acts as a fictional magnetic field, and is responsible for the anomalous transport. It is odd under the time reversal operation and even under the IS operation [37]. Therefore, to obtain a resultant non-zero Berry curvature, one needs to break either Time reversal symmetry (TRS) or Inversion Symmetry (IS) or both. Magnetic materials naturally exhibit the

TRS breaking, and the non-centrosymmetric systems have breaking IS, which might be the ideal candidate for the study of the Anomalous transport phenomena [38]. Numerous studies on magnetic Heusler alloys exist in the literature, only a limited number address the TRS breaking criterion linked with Berry curvature and the associated anomalous transport behaviour. Co_2CrAs and Co_2CrSb are types of Co-based magnetic full Heusler alloys. Rai et al. [39] theoretically predicted both materials as Ferromagnetic half Metallic system. However, their Anomalous transport behaviour, led by the Berry curvature feature on these materials, is unexplored yet. To fill this gap, motivated by this, this study systematically presents a computational prediction of the Berry curvature-driven AHE and ANE in the Magnetic Heusler alloys.

3.2 Computational Details

The first-principles calculations were performed to investigate the electronic, magnetic, Topological and transport properties of Heusler alloy. Density functional theory (DFT) is used which is implemented in the Vienna ab initio simulation package (VASP), employing the projector augmented-wave (PAW) method [34-36]. Further, the exchange-correlation effects were treated within the generalized gradient approximation (GGA+U) using the Perdew-Burke-Ernzerhof (PBE) functional, where calculated Hubbard U and exchange J parameters were approximately 3.94 and 0.81 eV for cobalt (Co), [37]. In order to perform spin-polarized calculations and structural optimization, a convergence criterion for the self-consistent field energy of 10^{-5} eV was set. For the plane wave basis, the energy cut-off value was set to 520 eV. A fully optimized Γ-centred k-mesh grid of 11 × 11 × 11 was used. For a full relativistic

approach, we also include the effect of spin-orbital coupling and consider magnetisation along (001) plane. Further, using maximally localized Wannier functions (MLWFs), we constructed a tight-binding Hamiltonian by Wannier90 code. The WannierTools package was used to calculate the transport properties and identify the Weyl nodes within the bulk electronic structure, as well as the surface Fermi arc, thereby confirming the topological nature of the system [39]. In addition, the Berry curvature distributions are calculated using the Kubo formulation as given equation 3.1. The AHC and ANC were evaluated using WannierTools with a dense 200×200×200 k-mesh for high precision using the given equations 3.2 and 3.3, respectively [40,14].

3.3 Structural Properties

The structural properties, including stable structural phase and lattice constant for Co_2CrAs and Co_2CrSb Heusler alloys, are computed by the structural optimization curve. Heusler alloys with the chemical formula X_2YZ typically crystallize in the cubic $L2_1$ structure ($AlCu_2Mn$ prototype), where X and Y refer to transition-metal elements, and Z refer to groups III, IV, or V of the periodic table. The $L2_1$ phase is centrosymmetric, meaning it preserves inversion symmetry. In this arrangement, the X atoms occupy the (0.25, 0.25, 0.25) and (0.75, 0.75, 0.75) Wyckoff sites, while the Y and Z atoms reside at (0.5, 0.5, 0.5) and (0, 0, 0), respectively, as illustrated in Fig. 1(a) and (b). However, Xa another structural phase also exist in the X_2YZ stoichiometry, with the similar Wyckoff positions, which can be achieved by replacing one X atomic position with the Y atom, in the $L2_1$ structure and vice versa [33,34]. Fig. 1 (c) and (d) curve represents the

variation in ground state energy of a conventional unit cell with respect to the lattice constant. For Co_2CrAs and Co_2CrSb, the calculated energy separation between the $L2_1$ and Xa structural configurations is 0.87 eV and 3.49 eV, respectively. These values demonstrate that, in both compounds, the $L2_1$ structure is energetically more favourable than the Xa phase. Further, the optimized lattice constant correspond to the minimum energy are found to be 5.78 Å and 6.00 Å for Co_2CrAs and Co_2CrSb Heusler alloys, respectively, which is well in agreement with the previously reported results, also listed in Table I [26–28,35]. Due higher energetic stability in $L2_1$ phase over Xa, we consider $L2_1$ structural phase for all further calculations.

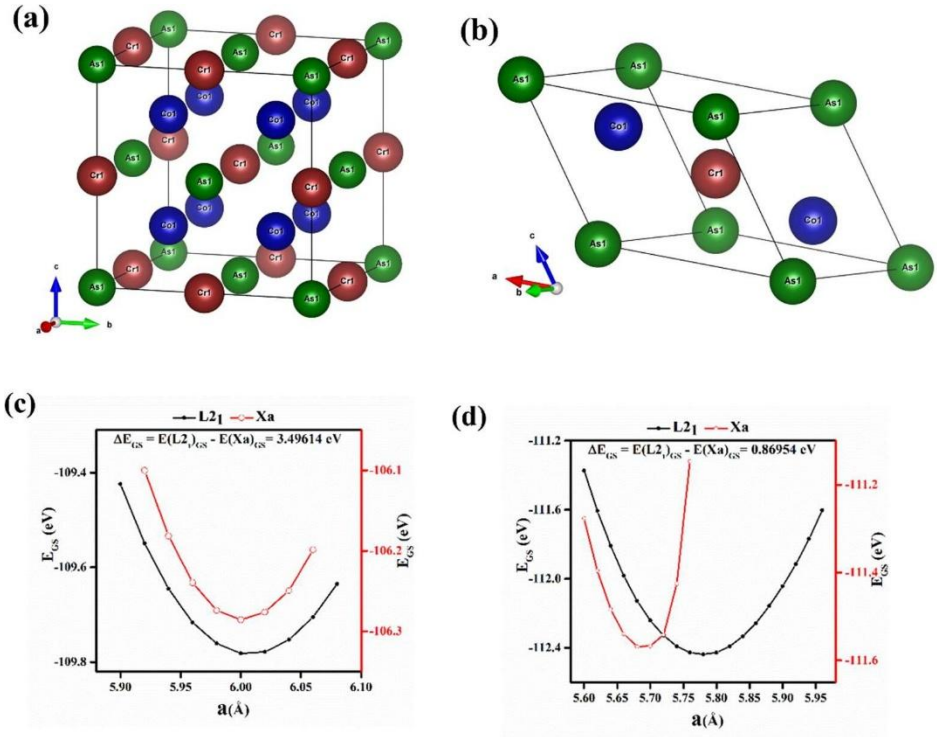

Figure 4:(a) Conventional unit cell of the Co_2CrZ (Z = As, Sb) Heusler alloys containing 16 atoms, with four atoms of each constituent element. (b) Corresponding

primitive unit cell comprising four atoms, one from each element. (c) and (d) the phase stability optimization curve in both $L2_1$ and Xa phases, between Ground state energy (EGS) with varying lattice constant a (Å) for Co_2CrAs and Co_2CrSb Heusler alloys respectively.

Table 1:Optimizes Lattice constants a (Å) and total magnetic moment (μB) for Co_2CrAs and Co_2CrSb Heusler alloy.

Heusler Alloy	Lattice constant a(Å)	Total magnetic moment (μB)
Co_2CrAs	5.78*, 5.78[#], 5.81[@], 5.79[$]	5.00*, 5.00[#], 4.82[@], 5.01[$]
Co_2CrSb	6.00*, 6.00[#], 5.99[δ]	5.00*, 5.00[#], 4.94[δ]

*this work, [#][26], [@][27], [$][35], and [δ][28]

To ascertain the dynamic stability of the structures in the $L2_1$ phase, we also performed a calculation of phonon dispersion for both alloys. As illustrated in Fig. 2, the phonon dispersion bands are plotted against the high symmetry path *Γ-X-U/K-Γ-L-W-X* in the BZ. The phonon dispersion spectra carrying the total 12 phonon branches corresponding to the four atoms per unit cell as shown in Figure 2(a) and (b) for Co_2CrAs and Co_2CrSb Heusler alloys. For these alloys, we do not observe any negative frequency phonon branches, which ensure the dynamical stability of both Heusler alloys in the magnetic phase.

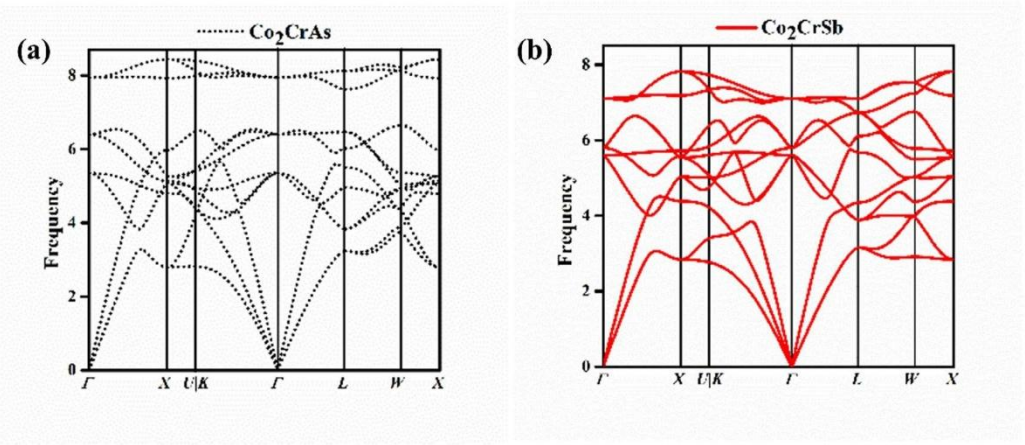

Figure 5: Phonon dispersion spectra along the high- symmetric k-path for (a) Co_2CrAs and (b) Co_2CrSb Heusler alloys.

3.4 Electronic, Magnetic, and Topological properties

To compute the magnetic nature and half-metallicity, the spin-polarized Density of states (DOS) and electronic bandstructure are calculated for both alloys. Fig. 3(a and b) display the total and partial DOS plot, which shows that the main Co-d, Cr-d, and As/Sb-p orbitals contribute near the Fermi level in both spin channels. In addition, the absence of electronic states at the Fermi level in the minority spin channel indicates the half-metallic nature of both Heusler alloys. Fig.3 (c and d) illustrates the spin-polarized electronic bandstructure for the Co_2CrAs and Co_2CrSb Heusler alloys, respectively. The minority spin states exhibit a clear semiconducting energy gap of value 0.39(0.28) eV for Co_2CrSb (Co_2CrSb) alloy. However, the majority spin states cross E_F and form a conducting channel between conduction and valence bands, which further confirms the half-metallic nature of both alloys. In addition to evaluating the magnetic properties of the

alloys, we also calculate the magnetic moment against all atoms present in the unit cell. Both the alloys exhibit ferromagnetic behaviour with a net magnetic moment value of 5 μB, which is also given in Table 1, and compared with the previously reported results.

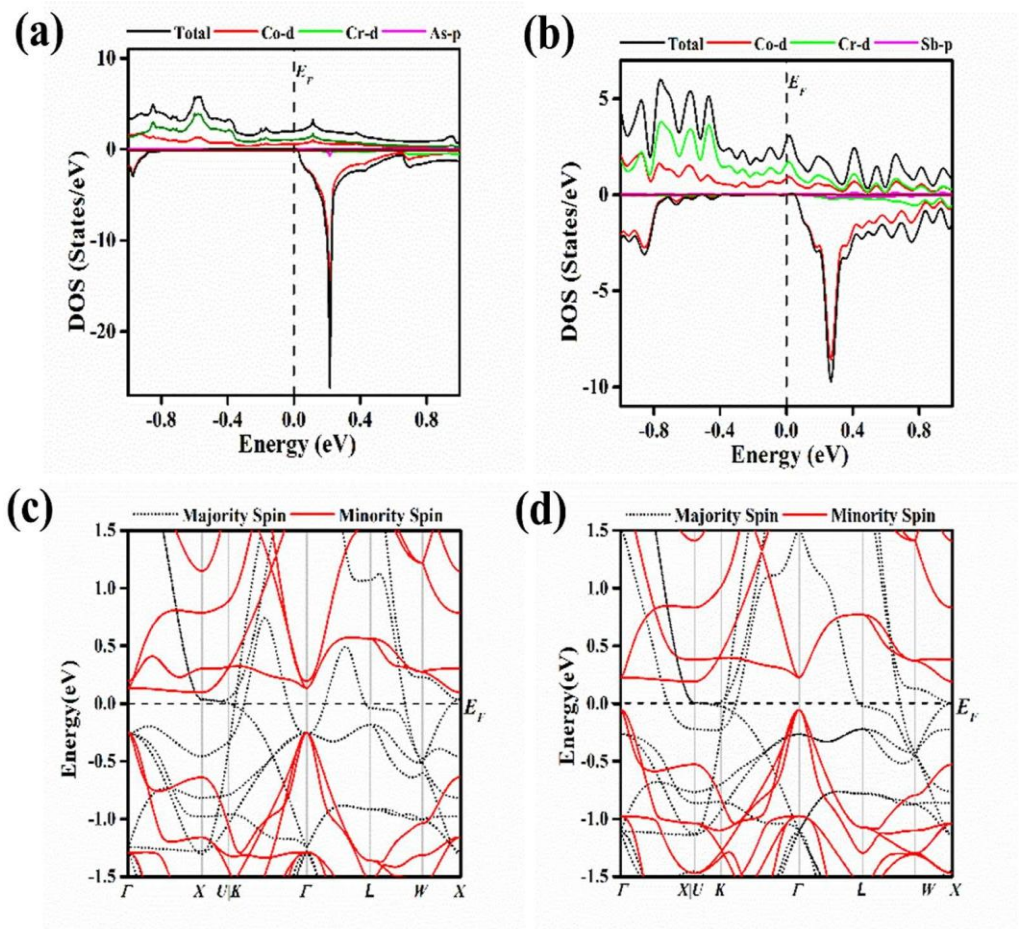

Figure 6: Spin Polarized total and partial Density of states (DOS) for (a) Co_2CrAs and (b) Co_2CrSb. Spin Polarized electronic bandstructure along the high symmetry k-path, for (c) Co_2CrAs and (d) Co_2CrSb Heusler alloys.

3.5 Berry Curvature, Anomalous Hall and Anomalous Nernst Effect

Berry curvature analysis characterizes the geometrical (Berry) phase associated with electronic wave-functions in momentum space and is described by the phase shift acquired by a wave-function during cyclic evolution in k-space. It is evaluated using the Kubo formalism in conjunction with a tight-binding Hamiltonian constructed from the Wannier90 code, and can be expressed as follows [10,36,37]:

$$\Omega_{ij}^{n}(k) = \sum_{n \neq m} \frac{\langle n|\frac{\partial H}{\partial k_i}|m\rangle\langle m|\frac{\partial H}{\partial k_j}|n\rangle - (i \leftrightarrow j)}{(E_n - E_m)^2} \quad (3.1)$$

Where $\Omega_{ij}^{n}(k)$ is Berry curvature ijcomponent of the nth band.ε_n andε_m are the energy eigenvalues of the Hamiltonian H corresponding to the $|n\rangle$ and $|m\rangle$ eigenstates, respectively, the energy eigenvalue of the Hamiltonian *H*.

Fig. 4 displays the electronic band structures (upper panels) and the corresponding Berry curvature distributions (lower panels) for Co_2CrAs and Co_2CrSb Heusler alloys in the presence of SOC. When SOC is included, spin ceases to be a good quantum number, and the two spin channels must be treated collectively. Around the E_F, SOC take care of the band degeneracy and induces energy gaps between previously degenerate bands over a narrow k-path region. These SOC-split bands contribute

significantly to the Berry curvature when one of the split bands is occupied, and the other remains unoccupied. In contrast, pairs of states that are either both occupied or both unoccupied provide only a minor contribution to the overall Berry curvature [15,35,43–46].

Fig. 4(a) shows the Berry curvature profile for Co_2CrAs, where a pronounced peak and several weaker features are observed along the k-path (lower panel). To identify the initial phase of these peaks, an enlarged of the SOC-included band structure near E_F is presented alongside the Berry curvature. The dominant peaks arise from SOC-induced energy gaps between nearly degenerate electronic bands within a narrow k-region, as clearly seen in the enlarged view of Fig. 4(b). The smaller peaks share a similar origin; however, their smaller magnitude is attributed to comparatively larger energy separations between the interacting bands as from equation 3.1. Additionally, the small dip in Berry curvature around the Γ point results from aligned electronic states that are both occupied, leading to a suppressed Berry curvature amplitude.

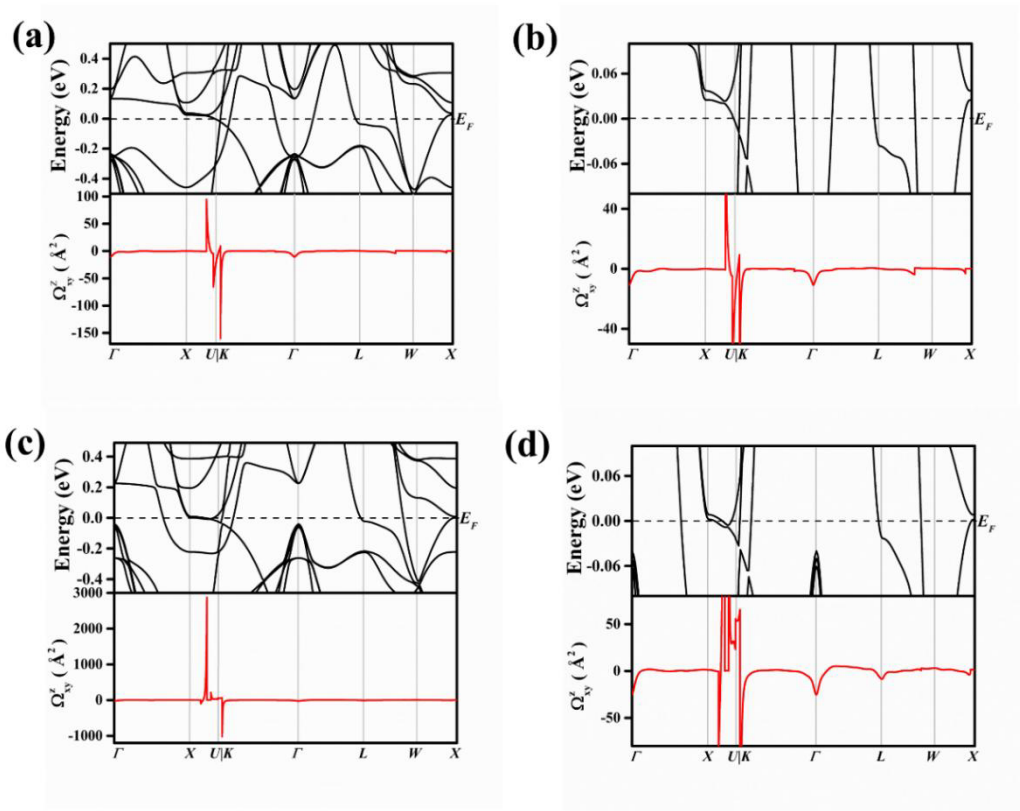

Figure 7: (a) Berry curvature feature (bottom channel) corresponding to electronic band-structure (lower channel) with SOC along the high-symmetry k-path for (a) Co_2CrAs and (c) Co_2CrSb. (b) and (d) is the magnified view of Berry curvature with bandstructure for (a) Co_2CrAs and (c) Co_2CrSb Heusler alloys, respectively.

For Co_2CrSb, as illustrated in Fig. 4 (c), three prominent peaks are observed, one positive and two negatives. These major Berry curvature peaks originate from SOC-induced energy gaps between electronic states near E_F within a confined k-region. The enlarged view in Fig. 4(d) reveals a minor dip near the Γ point with relatively small magnitude, which arises from electronic states situated below E_F that remain occupied. A comparison between the two alloys indicates that Co_2CrSb exhibits larger Berry curvature peaks than Co_2CrAs. This difference is attributed to the position of the SOC-gapped electronic states: in Co_2CrSb, these states lie directly at E_F, whereas in Co_2CrAs

they are positioned slightly above E_F, resulting in a comparatively weaker Berry curvature response.

Next, the AHC (σ_{xy}^{A}) is determined from the Berry curvature $\Omega_{ij}^{n}(k)$ using the following expression [47,48]:

$$\sigma_{xy}^{A} = \frac{-e^2}{\hbar} \int_{BZ} \frac{d^3k}{(2\pi)^3} f(k) \Omega_{ij}^{n}(k) \qquad (3.2)$$

The AHC for both Heusler alloys was calculated using Eq. 3.2 and plotted as a function of energy within ±1000 meV around the E_F, as shown in Fig. 5(a). For Co_2CrAs, the AHC is -309.67 S cm^{-1} at fermi-energy and reaches a maximum of 584.38 S cm^{-1} at 0.13 eV above E_F, which is approximately 1.8 times larger than its value at E_F. Similarly, for Co_2CrSb, the AHC is -167.26 S cm^{-1} at fermi-energy and attains a maximum magnitude of -668.99 S cm^{-1} at 0.97 eV below fermi-energy, nearly five times greater than its value at the fermi-energy. Hence, a slight shift in the E_F can significantly enhance the AHC. Such a shift can be achieved through appropriate chemical doping or by applying lattice strain, thereby enabling larger AHC values. These negative AHC values indicate that regions of positive Berry curvature dominate

the overall response. These substantial values of AHC obtained for these Heusler alloys are comparable to previously reported results.

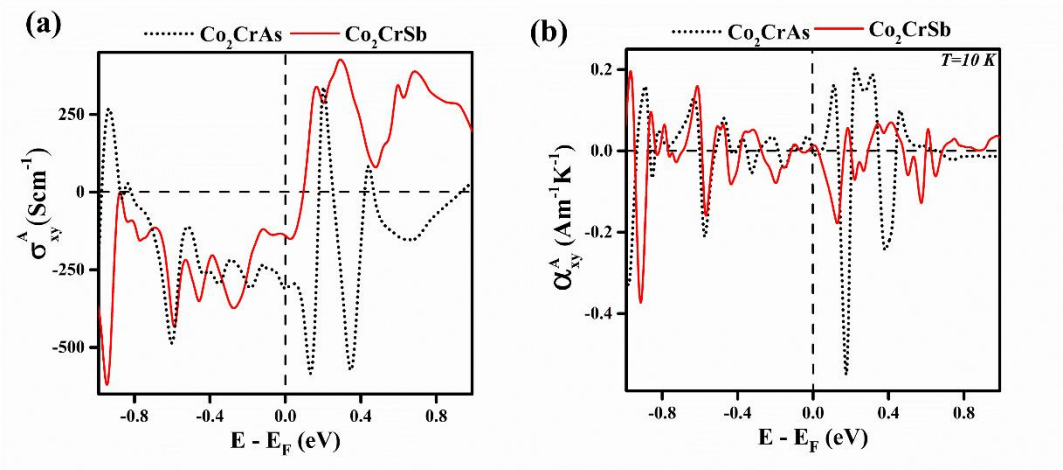

Figure 8: (a) Anomalous Hall conductivity with varying energy in the vicinity of Fermi level at 0 K and (b) Anomalous Nernst conductivity with varying energy in the vicinity of Fermi level at low temperature (10 K) for both Co_2CrAs and Co_2CrSb Heusler alloys.

Now AHC the thermoelectric counterpart, the *ANC* (α_{xy}^{A}), calculated as proposed by Xia et al. [4,54], can be expressed as:

$$\alpha_{xy}^{A}(T,\mu) = -\frac{1}{e}\int_{BZ} d\varepsilon \frac{\partial f(\varepsilon-\mu,T)}{\partial \varepsilon}\frac{\varepsilon-\mu}{T}\sigma_{xy}^{A}(\varepsilon) \qquad (3.3)$$

And at low temperature, the Mott relation is used to calculate the *ANC* (α_{xy}^{A}), and can be obtained from AHC, as from the equation [10,55,56]:

$$\alpha_{xy}^{A}(T,\mu) = -\frac{\pi^2}{3}\frac{k_B^2}{e}\frac{\partial \sigma_{xy}^{A}}{\partial \varepsilon}(\varepsilon_F) \qquad (3.4)$$

Where f(k) stands for the Fermi-Dirac distribution function, k_B is the Boltzmann constant, μ is the chemical potential, $\hbar$ is the reduced Planck constant, and integration is over the Brillouin zone. e is the electronic charge, and T is the actual temperature.

At low temperature (T = 0 K), the ANC calculated from the Mott relation given by equation 4, which is the energy derivative of the AHC. The ANC as a function of energy in the vicinity of E_F within ±1000 meV for both alloys is shown in Fig. 5(b). At T = 10 K, the Co_2CrAs alloy exhibits an ANC of 0.001 $Am^{-1}K^{-1}$ at E_F, which reaches a maximum value of -0.55 $Am^{-1}K^{-1}$ at 0.17 eV above the E_F. Similarly, for Co_2CrSb, the ANC is 0.013 $Am^{-1}K^{-1}$ at E_F and attains a maximum of -0.37 $Am^{-1}K^{-1}$ at 0.91 eV below E_F. These results indicate that even a slight shift in the chemical potential can lead to a substantial variation in the ANC.

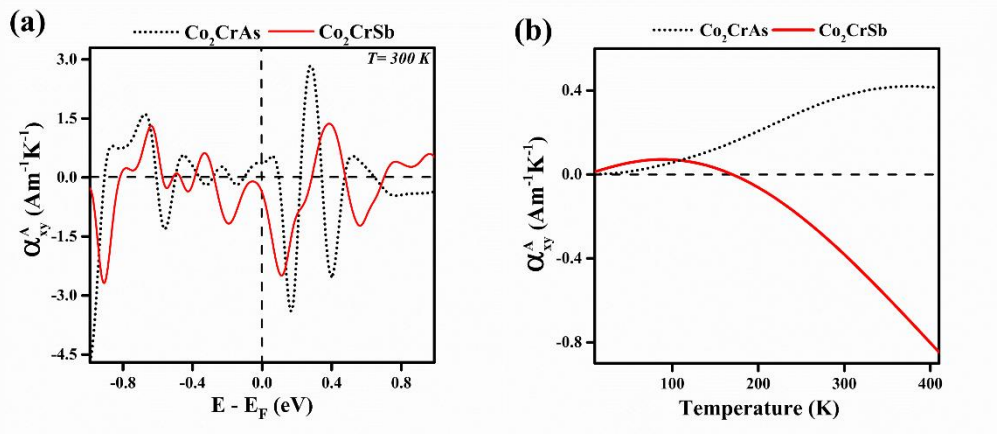

Figure 9: (a) Anomalous Nernst conductivity with varying energy in the vicinity of Fermi level at room temperature (300 K) and (b) Anomalous Nernst conductivity with the varying temperature at EF for both Co_2CrAs and Co_2CrSb Heusler alloys.

For potential room-temperature applications, the ANC was further evaluated from equation 3 at T = 300 K, plotted in Fig. 6(a). At the E_F, Co_2CrAs and Co_2CrSb exhibit

ANC values of 0.37 and 0.38 $Am^{-1}K^{-1}$, respectively. Upon shifting the E_F to -0.99 eV for Co_2CrAs and -0.90 eV for Co_2CrSb, the ANC reaches maximum values of -4.71 and -2.68 $Am^{-1}K^{-1}$, respectively. These values are approximately 13 and 7 times larger than those at the E_F. The enhanced ANC observed in these Heusler alloys is comparable to previously reported results for other ferromagnetic Heusler compounds [12,19,50,57–59].

We further computed the temperature dependence of the ANC at the E_F, as shown in Fig. 6(b). For Co_2CrAs, the ANC increases monotonically with temperature, reaching 0.37 $Am^{-1}K^{-1}$ at 300 K. However, Co_2CrSb maintains comparable larger values than Co_2CrAs throughout the investigated temperature range and exhibits a parabolic behaviour, attaining a maximum of 0.82 $Am^{-1}K^{-1}$ at 400 K. The observed variation of ANC with increasing temperature can be attributed to the interplay between thermal broadening effects and sharply peaked features in the Berry curvature [60]

CHAPTER 4

CONCLUSIONS AND FUTURE SCOPE

4.1 Conclusion

The present study explored anomalous transport phenomena in the new Co-based ferromagnetic Heusler alloys, Co_2CrAs and Co_2CrSb, by utilizing the Density functional theory, followed by green function approach. These are half-metallic systems, stable in the $L2_1$ structural phase, and possess a net magnetic moment of value 5 μ_B. The total and projected density of states revealed that the *d* orbitals of *Co* and *Cr* atoms and the *p* orbitals of *As/Sb* atom are mainly contributed to both spin channels and in the conduction and valence bands near the E_F. The spin-orbital coupling removes the degeneracy of degenerate electronic bands, in which those lying at the E_F contribute to the resultant Berry curvature. The observed net non-zero Berry curvature in both alloys further leads to the large AHC and ANC results. We observed the AHC value at T=0 K about 584.38 Scm^{-1} and -668.99 Scm^{-1} for Co_2CrAs and Co_2CrSb Heusler alloy, respectively. Further, the ANC at low temperature appears to be very small, but at room temperature, we observed large values -4.71 and -2.68 $Am^{-1}K^{-1}$ for Co_2CrAs and Co_2CrSb Heusler alloy, respectively. The variation in the ANC with the temperature is the consequence of the collective effect of thermal boarding and sharply peaked Berry curvature. Our findings for anomalous transport led by the Berry curvature in the new Co-based ferromagnetic Heusler alloys, making them a potential candidate for thermoelectric and new emerging quantum technological applications.

4.2 Future Scope

This work present theoretical understanding of the AHC and the ANC of Co_2CrAs and Co_2CrSb and opens many doors for future research. The theory people can explore the effect of external parameter as atomic disorder on electronic structure and chemical doping. This type of change can shift the fermi energy level and can enhance Berry curvature, AHC and ANC. In other hand Experimentalist can synthesis and do characteristic of Co_2CrAs and Co_2CrSb to confirm theoretical prediction. X-ray diffraction (XRD), transport measurements, scanning electron microscopy (SEM), and magnetic characterization experimental techniques can be used to investigate structural stability, magnetic properties, and anomalous Hall and Nernst responses. In addition future studies can explore topological phase transitions, nodal line structures, Weyl nodes, and symmetry-breaking mechanisms in Co-based Heusler alloys. In an application perspective, experimentalist can investigate Heterostructure fabrication and thin film Growth for Practical Application in sensor, spintronics and quantum technology.

Recently, Artificial Intelligence (AI) and Machine Learning (ML) techniques are usefull in material science. ML can predict electronic, magnetic, and topological properties of many Heusler compounds using material databases. This reduce computational cost and accelerate the discovery of materials having large anomalous Hall and Nernst Conductivity. Furthermore, deep learning can be used to identify new Heusler compounds with desirable Berry curvature. Such approaches will provide a faster way toward discovering next-generation materials for quantum, spintronic, and thermoelectric applications.

References

1. C. Fu, Y. Sun, and C. Felser, APL Mater. **8**, (2020).

2. S. A. Sofi and D. C. Gupta, J. Solid State Chem. **284**, 121178 (2020).

3. M. Zhong, N. T. T. Vu, W. Zhai, J. R. Soh, Y. Liu, J. Wu, A. Suwardi, H. Liu, G. Chang, K. P. Loh, W. Gao, C. Qiu, J. K. W. Yang, and Z. Dong, Adv. Mater. **37**, (2025).

4. N. Nagaosa, J. Sinova, S. Onoda, A. H. MacDonald, and N. P. Ong, Rev. Mod. Phys. **82**, 1539 (2010).

15. K. Manna, Y. Sun, L. Muechler, J. Kübler, and C. Felser, Nat. Rev. Mater. **3**, 244 (2018).

6. S. Yadav, Sangeeta, K. Kumar, and M. Singh, Phys. Lett. A **551**, 130625 (2025).

7. X. Zhou, H. Liu, W. Wu, K. Jiang, Y. Shi, Z. Li, Y. Sui, J. Hu, and J. Luo, Phys. Rev. B **105**, 205104 (2022).

8. A. Togo and I. Tanaka, Scr. Mater. **108**, 1 (2015).

9. A. A. Mostofi, J. R. Yates, Y.-S. Lee, I. Souza, D. Vanderbilt, and N. Marzari, Comput. Phys. Commun. **178**, 685 (2008).

10. Q. Wu, S. Zhang, H.-F. Song, M. Troyer, and A. A. Soluyanov, Comput. Phys. Commun. **224**, 405 (2018).

11. E. Wang, H. Zeng, W. Duan, and H. Huang, Phys. Rev. Lett. **132**, 266802 (2024).

12. K. Kumar, Sangeeta, R. Kumar, R. Kumar, M. Singh, and M. K. Kashyap, Adv. Theory Simulations (2025).

13. S. Chatterjee, J. Sau, S. Ghosh, S. Samanta, B. Ghosh, M. Kumar, and K. Mandal, J. Phys. Condens. Matter **35**, 035601 (2023).

14. M. Singh, H. S. Saini, J. Thakur, A. H. Reshak, and M. K. Kashyap, J. Solid State Chem. **208**, 71 (2013).

15. D. Xiao, Y. Yao, Z. Fang, and Q. Niu, Phys. Rev. Lett. **97**, 026603 (2006).

16. S. N. Guin, K. Manna, J. Noky, S. J. Watzman, C. Fu, N. Kumar, W. Schnelle, C. Shekhar, Y. Sun, J. Gooth, and C. Felser, NPG Asia Mater. **11**, 16 (2019).

17. T. Graf, C. Felser, and S. S. P. Parkin, Prog. Solid State Chem. **39**, 1 (2011).

18. J. Noky, Y. Zhang, J. Gooth, C. Felser, and Y. Sun, Npj Comput. Mater. **6**, 77 (2020).

20. B. Kakati, P. Saha, S. Alom, and M. B. Sahariah, J. Appl. Phys. **136**, (2024).

21 Zhijun Wang, MG Vergniory, S Kushwaha, Max Hirschberger, EV Chulkov, A Ernst, Nai Phuan Ong, Robert J Cava, and B Andrei Bernevig. Time-reversal-breaking Weyl fermions in magnetic Heusler alloys. Phys. Rev. Lett., 117(23):236401, 2016.

22 Takashi Kono, Masaaki Kakoki, Tomoki Yoshikawa, Xiaoxiao Wang, Kazuki Goto, Takayuki Muro, RieYUmetsu, andAkioKimura. Visualizinghalf-metallic bulk band struc ture with multiple Weyl cones of the Heusler ferromagnet. Phys. Rev. Lett., 125(21):216403, 2020.

23 Enke Liu, Yan Sun, Nitesh Kumar, Lukas Muechler, Aili Sun, Lin Jiao, Shuo-Ying Yang, Defa Liu, Aiji Liang, Qiunan Xu, et al. Giant anomalous Hall effect in a ferromagnetic kagome-lattice semimetal. Nat. Phys, 14(11):1125–1131, 2018.

24 Satya N Guin, Kaustuv Manna, Jonathan Noky, Sarah J Watzman, Chenguang Fu, Nitesh Kumar, Walter Schnelle, Chandra Shekhar, Yan Sun, Johannes Gooth, et al. Anomalous

Nernst effect beyond the magnetization scaling relation in the ferromagnetic Heusler com pound Co2MnGa. NPG Asia Materials, 11(1):16, 2019.

25 Gaurav K Shukla, Jyotirmoy Sau, Nisha Shahi, Anupam K Singh, Manoranjan Kumar, and Sanjay Singh. Anomalous hall effect from gapped nodal line in the Co2FeGe Heusler com pound. Phys. Rev. B, 104(19):195108, 2021.

26 Jonathan Noky, Johannes Gooth, Claudia Felser, and Yan Sun. Characterization of topolog ical band structures away from the fermi level by the anomalous Nernst effect. Phys. Rev. B., 98(24):241106, 2018

27 Gaurav K Shukla, Ujjawal Modanwal, and Sanjay Singh. Nodal-line symmetry breaking induced colossal anomalous hall and Nernst effects in Cu2CoSn Heusler compound. Appl. Phys. Lett., 123(5), 2023.

28 Enke Liu, Yan Sun, Nitesh Kumar, Lukas Muechler, Aili Sun, Lin Jiao, Shuo-Ying Yang, Defa Liu, Aiji Liang, Qiunan Xu, et al. Giant anomalous Hall effect in a ferromagnetic kagome-lattice semimetal. Nat. Phys, 14(11):1125–1131, 2018.

29 Kelvin Elphick, William Frost, Marjan Samiepour, Takahide Kubota, Koki Takanashi, Hi roaki Sukegawa, Seiji Mitani, and Atsufumi Hirohata. Heusler alloys for spintronic devices: review on recent development and future perspectives. STAM, 22(1):235–271, 2021.

30 J Kübler, GH Fecher, and C Felser. Understanding the trend in the curie temperatures of Co2-based Heusler compounds: Ab initio calculations. Phys. Rev. B., 76(2):024414, 2007.

31. M. Kohmoto, Ann. Phys. (N. Y). **160**, 343 (1985).

32. B. K. Hazra, M. M. Raja, R. Rawat, A. Lakhani, S. N. Kaul, and S. Srinath, J. Magn. Magn. Mater. **448**, 371 (2018).

33. A. Sharma, S. Javvaji, L. Kowachi, A. PATTNAIK, H. Sinha, S. Arokiasamy, C. Prashanth, M. Chou, S.-M. Huang, and P. Rambabu, J. Phys. Condens. Matter (2026).

34. W. Kohn and L. J. Sham, "Self-consistent equations including exchange and correlation effects," Phys. Rev., vol. 140, no. 4A, pp. A1133–A1138, Nov. 1965, doi: 10.1103/PhysRev.140.A1133.

35. J. P. Perdew, K. Burke, and M. Ernzerhof, "Generalized gradient approximation made simple," Phys. Rev. Lett., vol. 77, no. 18, pp. 3865–3868, Oct. 1996, doi: 10.1103/PhysRevLett.77.3865.

36. G. K. Shukla, A. K. Jena, N. Shahi, K. K. Dubey, I. Rajput, S. Baral, K. Yadav, K. Mukherjee, A. Lakhani, K. Carva, S.-C. Lee, S. Bhattacharjee, and S. Singh, Phys. Rev. B **105**, 035124 (2022).

37. K. G, V. E, R. K, and N. K. T.R., Solid State Sci. **156**, 107679 (2024).

38. Q. Wu, S. Zhang, H.-F. Song, M. Troyer, and A. A. Soluyanov, Comput. Phys. Commun. **224**, 405 (2018).

39. D. P. Rai and R. K. Thapa, J. Alloys Compd. **542**, 257 (2012).

40. R. Karplus and J. M. Luttinger, Phys. Rev. **95**, 1154 (1954)

41. P. Sahu, S. Bhowal, and S. Satpathy, Phys. Rev. B **103**, 085113 (2021).

42. H. Yang, W. You, J. Wang, J. Huang, C. Xi, X. Xu, C. Cao, M. Tian, Z.-A. Xu, J. Dai, and Y. Li, Phys. Rev. Mater. **4**, 024202 (2020).

43. Y. Zhang, Y. Sun, and B. Yan, Phys. Rev. B **97**, 041101 (2018).

44. M. Born and K. Huang, *Dynamical Theory Of Crystal Lattices* (Oxford University PressNew York, NY, 1996).

45. C.-S. Man and M. Huang, J. Elast. **105**, 29 (2011).

46. Y. Yao, L. Kleinman, A. H. MacDonald, J. Sinova, T. Jungwirth, D. Wang, E. Wang, and Q. Niu, Phys. Rev. Lett. **92**, 037204 (2004).

47. D. J. Thouless, M. Kohmoto, M. P. Nightingale, and M. den Nijs, Phys. Rev. Lett. **49**, 405 (1982).

48. J. M. Luttinger, Phys. Rev. **112**, 739 (1958).

49. D. Xiao, M.-C. Chang, and Q. Niu, Rev. Mod. Phys. **82**, 1959 (2010).

50. C. Felser, L. Wollmann, S. Chadov, G. H. Fecher, and S. S. P. Parkin, APL Mater. **3**, 041518 (2015).

51. J. Sau, D. Sa, and M. Kumar, Electron. Struct. **6**, 015008 (2024).

52. K. Meliani, M. Dehbaoui, K. Djennane, and N. E. H. Dehimi, Phys. B Condens. Matter **694**, 416442 (2024).

53. G. K. Shukla, J. Sau, N. Shahi, A. K. Singh, M. Kumar, and S. Singh, Phys. Rev. B **104**, 195108 (2021).

54. Y. P. Mizuta and F. Ishii, in *Proc. Int. Conf. Strongly Correl. Electron Syst.* (Journal of the Physical Society of Japan, 2014).

55. W.-L. Lee, S. Watauchi, V. L. Miller, R. J. Cava, and N. P. Ong, Phys. Rev. Lett. **93**, 226601 (2004).

56. D. Xiao, Y. Yao, Z. Fang, and Q. Niu, Phys. Rev. Lett. **97**, 026603 (2006).

57. A. Sakai, Y. P. Mizuta, A. A. Nugroho, R. Sihombing, T. Koretsune, M.-T. Suzuki, N. Takemori, R. Ishii, D. Nishio-Hamane, R. Arita, P. Goswami, and S. Nakatsuji, Nat. Phys. **14**, 1119 (2018).

58. J. Xu, W. A. Phelan, and C.-L. Chien, Nano Lett. **19**, 8250 (2019).

59. A. Chanda, J. Nag, N. Schulz, A. Alam, K. G. Suresh, M.-H. Phan, and H. Srikanth, Phys. Rev. B **109**, 224415 (202)

PLAGIARISM REPORT

Satyam

28/07/26

DR. MUKHTIYAR SINGH
Supervisor
(Assistant Professor)

6	Mainak Dey Sarkar, Koushik Pradhan, Satyaki Kar, Debabrata Sinha, Dirtha Sanyal, Debnarayan Jana. "Tuning the Topological Properties of Heusler Alloys via Bandstructure Engineering", Journal of Physics: Condensed Matter, 2026 Publication	<1%
7	patents.google.com Internet Source	<1%
8	Submitted to University of Birmingham Student Paper	<1%
9	arxiv.org Internet Source	<1%
10	jlupub.ub.uni-giessen.de Internet Source	<1%
11	Wan, Mingyu. "Electrocatalysis Modulated by Organic-Inorganic Interfaces", University of Massachusetts Lowell, 2024 Publication	<1%
12	theses.hal.science Internet Source	<1%
13	Submitted to Anna University Student Paper	<1%
14	Jonathan Noky, Yan Sun. "Linear Response in Topological Materials", Applied Sciences, 2019 Publication	<1%
16	www.mdpi.com Internet Source	<1%

15	Submitted to Palestine Technical University Kadoorie Student Paper	<1%
16	edoc.ub.uni-muenchen.de Internet Source	<1%

AI REPORT

Satyam 222

ANC

Quick Submit

Quick Submit

Delhi Technological University

Document Details

Submission ID

trn:oid:::1:3580731883

Submission Date

May 28, 2026, 8:24 AM GMT+5:30

Download Date

May 28, 2026, 8:31 AM GMT+5:30

File Name

plag_report.docx

File Size

3.0 MB

31 Pages

5,917 Words

33,612 Characters

*% detected as AI

AI detection includes the possibility of false positives. Although some text in this submission is likely AI generated, scores below the 20% threshold are not surfaced because they have a higher likelihood of false positives.

Caution: Review required.

It is essential to understand the limitations of AI detection before making decisions about a student's work. We encourage you to learn more about Turnitin's AI detection capabilities before using the tool.

Disclaimer

Our AI writing assessment is designed to help educators identify text that might be prepared by a generative AI tool. Our AI writing assessment may not always be accurate (i.e., our AI models may produce either false positive results or false negative results), so it should not be used as the sole basis for adverse actions against a student. It takes further scrutiny and human judgment in conjunction with an organization's application of its specific academic policies to determine whether any academic misconduct has occurred.

COMMUNICATION RECORD

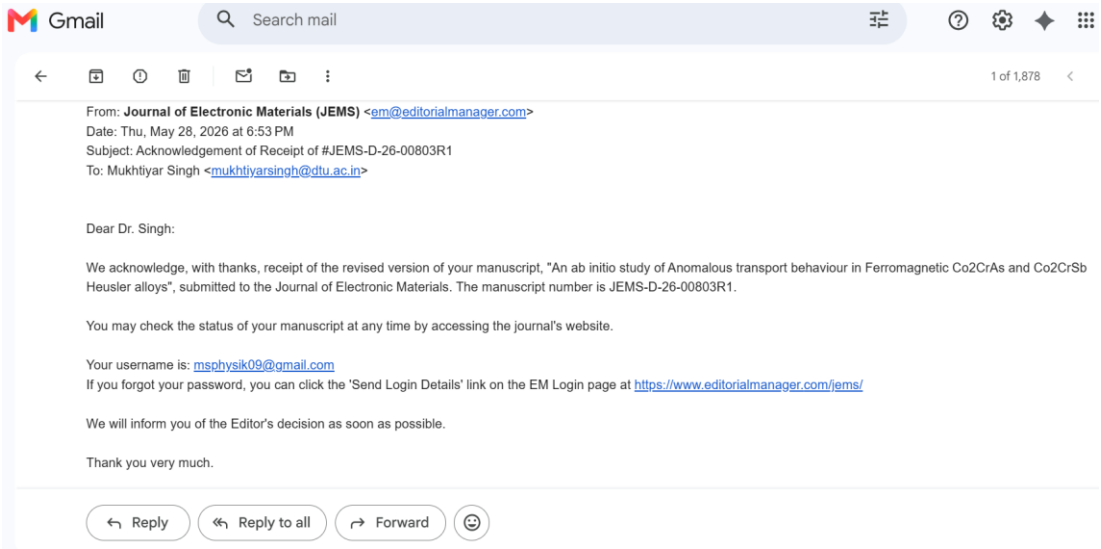

Gmail

Search mail

1 of 1,878

From: **Journal of Electronic Materials (JEMS)** <em@editorialmanager.com>
Date: Thu, May 28, 2026 at 6:53 PM
Subject: Acknowledgement of Receipt of #JEMS-D-26-00803R1
To: Mukhtiyar Singh <mukhtiyarsingh@dtu.ac.in>

Dear Dr. Singh:

We acknowledge, with thanks, receipt of the revised version of your manuscript, "An ab initio study of Anomalous transport behaviour in Ferromagnetic Co2CrAs and Co2CrSb Heusler alloys", submitted to the Journal of Electronic Materials. The manuscript number is JEMS-D-26-00803R1.

You may check the status of your manuscript at any time by accessing the journal's website.

Your username is: msphysik09@gmail.com
If you forgot your password, you can click the 'Send Login Details' link on the EM Login page at https://www.editorialmanager.com/jems/

We will inform you of the Editor's decision as soon as possible.

Thank you very much.

Reply | Reply to all | Forward

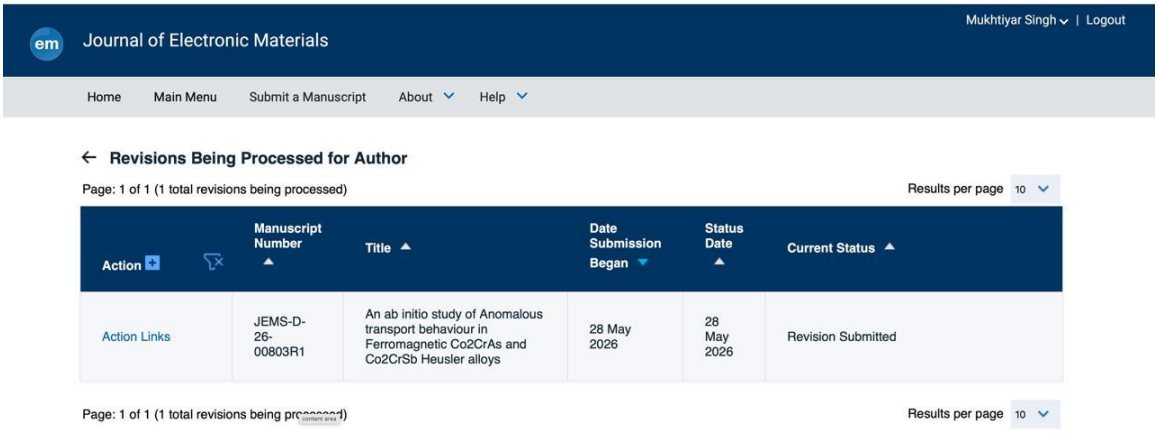

Journal of Electronic Materials

Mukhtiyar Singh | Logout

Home | Main Menu | Submit a Manuscript | About | Help

Revisions Being Processed for Author

Page: 1 of 1 (1 total revisions being processed)

Results per page 10

Action	Manuscript Number	Title	Date Submission Began	Status Date	Current Status
Action Links	JEMS-D-26-00803R1	An ab initio study of Anomalous transport behaviour in Ferromagnetic Co2CrAs and Co2CrSb Heusler alloys	28 May 2026	28 May 2026	Revision Submitted

Page: 1 of 1 (1 total revisions being processed)

Results per page 10

PROOF AND SCOPUS INDEXING

JOURNAL OF ELECTRONIC MATERIALS

Publisher: SPRINGER , ONE NEW YORK PLAZA, SUITE 4600 , NEW YORK, United States, NY, 10004

ISSN / eISSN: 0361-5235 / 1543-186X

Web of Science Core Collection: Science Citation Index Expanded

Additional *Web of Science* Indexes: Current Contents Electronics & Telecommunications Collection | Current Contents Physical, Chemical & Earth Sciences | Essential Science Indicators

Share This Journal | View profile page

* Requires free login.

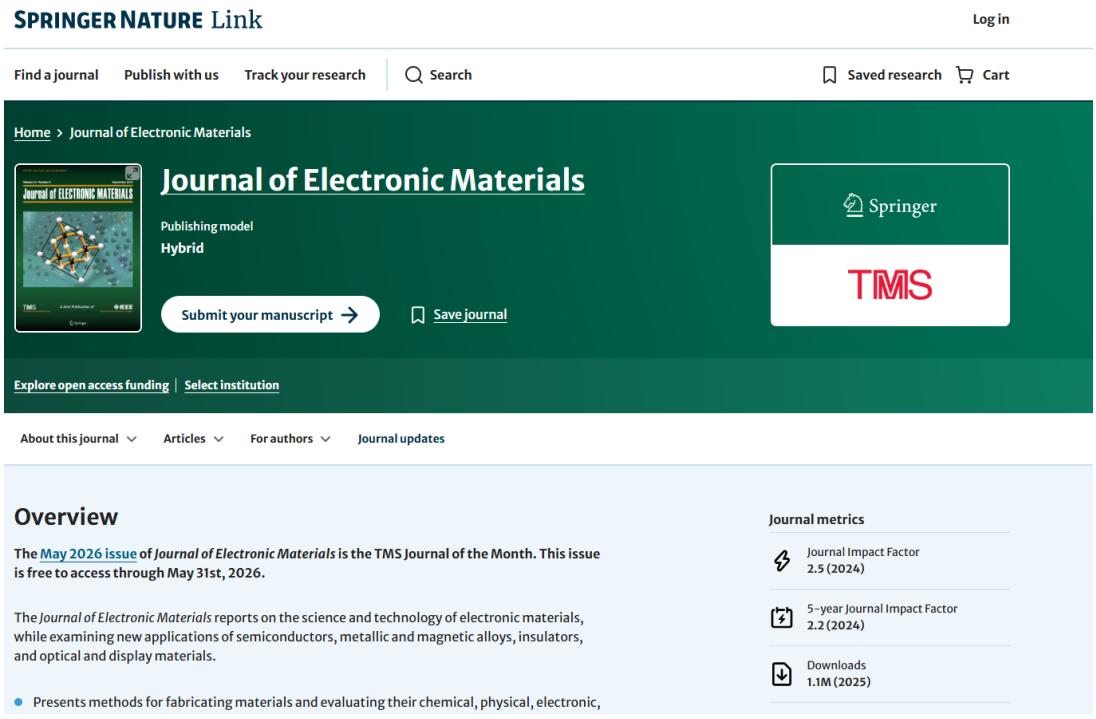

SPRINGER NATURE Link

Log in

Find a journal | Publish with us | Track your research | Search | Saved research | Cart

Home > Journal of Electronic Materials

Journal of Electronic Materials

Publishing model
Hybrid

Submit your manuscript | Save journal

Springer | TMS

Explore open access funding | Select institution

About this journal | Articles | For authors | Journal updates

Overview

The May 2026 issue of *Journal of Electronic Materials* is the TMS Journal of the Month. This issue is free to access through May 31st, 2026.

The *Journal of Electronic Materials* reports on the science and technology of electronic materials, while examining new applications of semiconductors, metallic and magnetic alloys, insulators, and optical and display materials.

- Presents methods for fabricating materials and evaluating their chemical, physical, electronic,

Journal metrics

Journal Impact Factor
2.5 (2024)

5-year Journal Impact Factor
2.2 (2024)

Downloads
1.1M (2025)

LIST OF CONFERENCE

1. Name of Conference: National Conference on Emerging Trends in Multifunctional Materials and Devices (NC-ETMMD-2026)

   Conference Dates: 11-12, March 2026

   Mode of the Conference: Offline

   Venue: JNU, New Delhi, India
2. Name of Conference: International Conference on Quantum Materials, ICQM-2026

   Conference Dates: 13-14, February 2026

   Mode of the Conference: Offline

   Venue: Svnit, Surat, India
3. Name of Conference: 5th International Conference on Recent Trends in Environment & Sustainable Development

   Conference Dates: 22-24, January 2026

   Mode of the Conference: Offline

   Venue: Vivekananda Global University, Jaipur, India

Anusandhan National Research Foundation

National Conference on Emerging Trends in Multifunctional Materials and Devices

(NC-ETMMD 2026)

Organized by

School of Physical Sciences, Jawaharlal Nehru University, New Delhi-110067 (India)

भौतिक विज्ञान संस्थान, जवाहरलाल नेहरू विश्वविद्यालय, नई दिल्ली-११००६७ (भारत)

11th-12th March 2026

Certificate of Appreciation

This is to certify that Prof./Dr./Mr./Ms./Mrs. Satyam Verma affiliated with Delhi Technological University, has presented a Poster titled An ab-initio study of Anomalous transport behaviour in Ferromagnetic Co_2CrPS and Co_2CrSb Heusler alloy in the "National Conference on Emerging Trends in Multifunctional Materials and Devices" held at Jawaharlal Nehru University, New Delhi, India, from 11th -12th March 2026.

Pritam Mukhopadhyay

Dean

Prof. Pritam Mukhopadhyay

Convenor

Dr. Arvind Kumar

1 of 1


सरदार वल्लभभाई राष्ट्रीय प्रौद्योगिकी संस्थान, सूरत
Sardar Vallabhbhai National Institute of Technology
Surat –395 007 (Gujarat), India
ICQM 2026
Certificate
This is to certify that Mr./Mrs./Prof./Dr. Satyam Verma from Delhi Technological University has attended / Oral presentation / Poster presentation given in the International Conference on Quantum Materials (ICQM-2026) Organized by Department of Physics, Sardar Vallabhbhai National Institute of Technology, Surat, during 13-14 February, 2026.
Organizing Secretary ICQM-2026
Convener ICQM-2026
Head Department of Physics
IOP Publishing
ICQM 2026
INTERNATIONAL CONFERENCE ON QUANTUM MATERIALS (ICQM-2026)
13-14 February, 2026
Best Poster Award
ICQM-2026
Department of Physics, SVNIT, Surat 395007, India


RTESD 2026
5th International Conference on
RECENT TRENDS IN ENVIRONMENT AND SUSTAINABLE DEVELOPMENT
(RTESD 2026)
Organized by: Department of Sciences, Vivekananda Global University, Jaipur
VGU
CERTIFICATE OF PARTICIPATION
This Certificate is Presented to
Mr. Satyam Verma
from
Delhi Technological University, New Delhi
for
Making Oral / Poster Presentation in the Confrence on Topic
A computational investigation of Anomalous Hall and Nernst effect in Co2CrSb, a Co-based Heusler alloy
Sponsored by:
Government of Rajasthan Department of Science & Technology
PROF. (DR.) SUBODH SRIVASTAVA
Conference Chair
22–24 January, 2026
Prof. (Dr.) Sushila
Head, Department of Sciences